Kalman filter based optimal control law for Star Oriented and Layer Oriented Multiconjugate Adaptive Optics

Le Roux B.[1], Ragazzoni R.[1], Arcidiacono C.[1], Conan J.-M.[2], Kulcsár C.[3], Raynaud H.-F.[3]
[1] Osservatorio Astrofisico di Arcetri (INAF),
Firenze, Italy
[2] Office National d'Études et de Recherches Aérospatiales (ONERA),
Châtillon, France
[3] Université Paris 13, Institut Galilée, L2TI,
Villetaneuse, France

ABSTRACT

We first recall in this paper the optimal closed loop control law for multiconjugate adaptive optics [MCAO]. It is based on a Kalman filter and a feedback control. The prior model on which is based the Kalman filter is developped in a state-space representation and the differences in the model between Star Oriented [SO] MCAO and Layer Oriented [LO] MCAO are presented. This approach allows to take into account the wavefront sensing noise, the turbulence profil model, the Kolmogorov statistics and a temporal model of the turbulence. Simulation results are given in SO MCAO and the Kalman based approach is compared to the more standard Optimized Modal Gain Integrator [OMGI].

Keywords: Multiconjugate Adaptive Optics, Star Oriented, Layer Oriented, Closed Loop, Kalman Filter.

1. INTRODUCTION

High resolution imaging with ground-based telescopes can now be reached with adaptive optics [AO]. However, classical adaptive optics, with a single deformable mirror [DM] in the pupil, allows to correct the turbulence only on a limited corrected field of view [FOV]. This effect comes from the volumic aspect of the atmospheric turbulence. Large FOV correction can therefore be obtained by correcting the volume of turbulence with several DM optically conjugated at various altitudes. This corresponds to the multi-conjugate adaptive optics [MCAO] concept. The measurement should allow to estimate the turbulence volume. There are two different possible approaches to estimate such a volume, both using several wavefront sensors [WFS]. In the Star Oriented [SO] approach, each WFS is dedicated to a guide star [GSs] and the volume of turbulence (meaning the turbulence in different altitudes) can be estimated from the measurements in the GSs directions [5–7]. In the Layer Oriented approach [9,17], the WFSs are not any more dedicated to directions but to altitudes. Each WFS is conjugated to a specific altitude and is looking to all stars. The volume of turbulence is then estimated from the measurements in different altitudes.

One key issue in an MCAO system is the estimation of the correction phases from the wavefront sensing data. We recall in section 3 the optimal approach for closed loop operation already proposed in [1] and in [4]. It uses spatial and temporal priors expressed in a state-space model formalism, a Kalman filter and a feedback control derived from the classical linear estimation theory [10–12]. We show how this general approach can be adapted to SO MCAO or LO MCAO just by changing the state-space model. We present in section 4 numerical simulations of the Kalman filter in SO MCAO and we compare its performance with those obtained with the Optimized Modal Gain Integrator [OMGI] [13,14] generalyzed to MCAO.

2. MCAO, SYSTEM DESCRIPTION AND NOTATIONS

Anisoplanatism comes from the volumic nature of the turbulence. A single mirror in the pupil cannot correct a volume of turbulence. If its shape is adapted to the turbulence in one direction, it can't correct efficently the turbulence away from the reference star. The concept of MCAO is based on the use of a volume of correction, meaning several mirrors conjugated to several altitudes, to correct the volume of turbulence.

Advancements in Adaptive Optics, edited by Domenico Bonaccini Calia, Brent L. Ellerbroek, Roberto Ragazzoni, Proceedings of SPIE Vol. 5490 (SPIE, Bellingham, WA, 2004)
0277-786X/04/$15 · doi: 10.1117/12.551422

Downloaded From: http://proceedings.spiedigitallibrary.org/ on 07/14/2015 Terms of Use: http://spiedl.org/terms

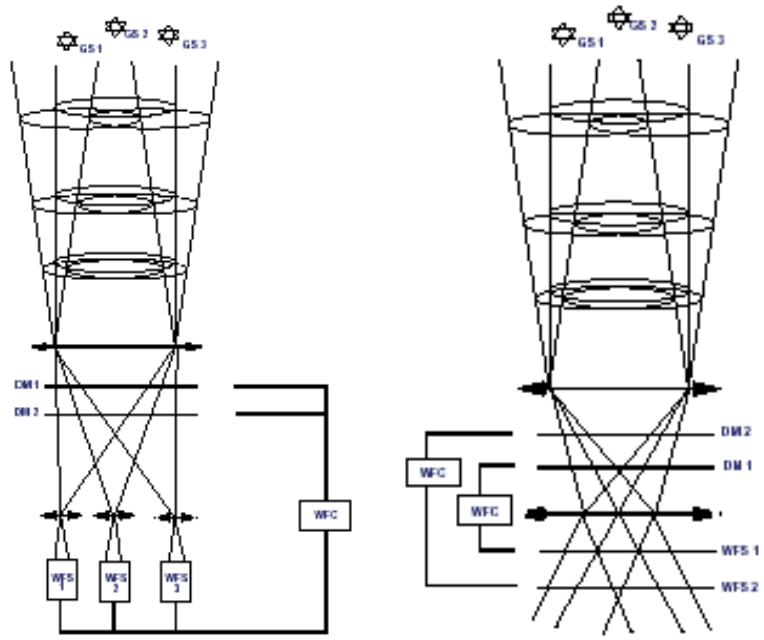

Figure 1. Left : representation of a Star Oriented MCAO system, each WFS is looking to one GS. Right : representation of a Layer Oriented MCAO system, each WFS is conjugated to a different altitude and looking to all the GSs.

We model the turbulent volume by N_L discrete independent turbulent layers located at altitudes $\{h_j\}_j$. We associate to each layer a turbulence strength $C_n^2(h_j)\delta h$, where $C_n^2(h_j)$ is the index structure constant in layer j and δh the thickness of the layer. This turbulent volume is corrected by N_{DM} deformable mirrors optically conjugated at altitudes $\{h'_j\}_j$. The turbulence statistics is assumed to be Kolmogorov for each turbulent layer.

The measurement of the turbulent volume is done with WFSs looking at reference stars called the Guide Stars [GSs]. In a SO MCAO system, as represented in Fig. 1 left, each WFS is in the pupil and looking to one GS whereas in a LO MCAO system, each WFS is conjugated to an given altitude and looking to all stars (as presented in Fig. 1 right).

We consider N_{gs} GSs in the $\boldsymbol{\beta} = \{\beta_i\}_{i=1}^{N_{gs}}$ directions. The field of view of interest, where the correction has to be optimized, is discretized into K angles and denoted $\boldsymbol{\alpha} = \{\alpha_i\}_{i=1}^{K}$.

We will use for the phase in the volume ϕ and the phase in the pupil φ a discrete representation based on a modal expansion of the phase, for instance the Zernike polynomials. The turbulent and correction phases $\boldsymbol{\phi}^{cor}$ and $\boldsymbol{\phi}^{tur}$ are then represented by vectors of coefficients: $\{\boldsymbol{\phi}_k^{cor}\}_k$, $\{\boldsymbol{\phi}_k^{tur}\}_k$. The turbulence is assumed to be Kolmogorov and the covariance matrix is given for the Zernike basis in [19]. In this representation, $\boldsymbol{\varphi}^{tur} = \{\boldsymbol{\varphi}^{tur,j}\}_j$ is the turbulent volumic phase in all layers and $\boldsymbol{\varphi}^{cor} = \{\boldsymbol{\varphi}^{cor,j}\}_j$ is the correction volumic phase generated by all the deformable mirrors. $\boldsymbol{\varphi}^{tur}$ is modelized as a stochastic centered variable of Gaussian statistics characterized by its covariance matrix $C_{\boldsymbol{\varphi}}$.

$\mathbf{M}_{\alpha_i}^{L,SO}$ is defined as the matrix which performs the sum of the contributions of each turbulent wavefront in the direction α_i. $\mathbf{M}_{\alpha_i}^{DM,SO}$ performs the sum of the contributions of each mirror in the direction α_i. The turbulent phase arriving on the pupil can therefore be written in function of the volumic phase as:

$$\boldsymbol{\phi}_{\alpha_i}^{tur} = \mathbf{M}_{\alpha_i}^{L,SO} \boldsymbol{\varphi}^{tur} \tag{1}$$

and the correction phase in the pupil as :

$$\boldsymbol{\phi}_{\alpha_i}^{cor} = \mathbf{M}_{\alpha_i}^{DM,SO} \boldsymbol{\varphi}^{cor}. \tag{2}$$

Downloaded From: http://proceedings.spiedigitallibrary.org/ on 07/14/2015 Terms of Use: http://spiedl.org/terms

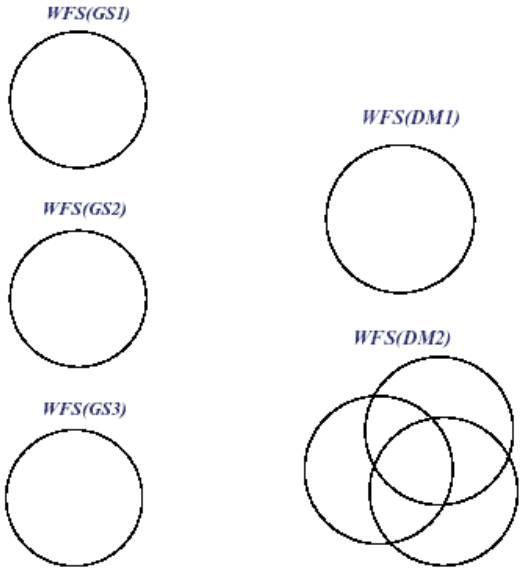

Figure 2. Illustration of the footprints of the pupils. On the left side, the SO MCAO case, the measurements are done in the pupil plane and in the direction of the three GSs. On the right side, the LO MCAO case, the WFSs are looking at all the GSs in the same time. The first measurement is done in the pupil plane and the second one at a given altitude.

We define $\mathbf{M}_{\boldsymbol{\alpha}}^{L,SO}$ as $\mathbf{M}_{\boldsymbol{\alpha}}^{L,SO} = \left((\mathbf{M}_{\alpha_1}^{L,SO})^T, \ldots, (\mathbf{M}_{\alpha_i}^{L,SO})^T, \ldots, (\mathbf{M}_{\alpha_{N_{gs}}}^{L,SO})^T\right)^T$, $\mathbf{M}_{\boldsymbol{\alpha}}^{L,SO}$ being the matrix which performs the sum of the contributions of each turbulent wavefront in all the directions $\boldsymbol{\alpha} = \{\alpha_i\}_i$:

$$\boldsymbol{\Phi}_{\boldsymbol{\alpha}}^{tur} = \{\boldsymbol{\phi}_{\alpha_i}^{tur}\}_i = \mathbf{M}_{\boldsymbol{\alpha}}^{L,SO} \boldsymbol{\varphi}^{tur}. \tag{3}$$

In the same way, $\mathbf{M}_{\boldsymbol{\alpha}}^{DM,SO}$ is the matrix performing the sum of the contributions of each DM in all the directions $\boldsymbol{\alpha} = \{\alpha_i\}_i$, which is written $\mathbf{M}_{\boldsymbol{\alpha}}^{DM,SO} = \left((\mathbf{M}_{\alpha_1}^{DM,SO})^T, \ldots, (\mathbf{M}_{\alpha_i}^{DM,SO})^T, \ldots, (\mathbf{M}_{\alpha_{N_{gs}}}^{DM,SO})^T\right)^T$.

These notations are also defined in the same way for β_i or $\boldsymbol{\beta}$ rather than α_i or $\boldsymbol{\alpha}$ so that Eq. (1), (2) and (3) can be written using $\mathbf{M}_{\beta_i}^{L,SO}$, $\mathbf{M}_{\beta_i}^{DM,SO}$, $\mathbf{M}_{\boldsymbol{\beta}}^{L,SO}$, $\mathbf{M}_{\boldsymbol{\beta}}^{DM,SO}$, $\boldsymbol{\phi}_{\beta_i}^{tur}$, $\boldsymbol{\Phi}_{\boldsymbol{\beta}}^{tur}$, $\boldsymbol{\phi}_{\beta_i}^{cor}$ and $\boldsymbol{\Phi}_{\boldsymbol{\beta}}^{cor}$.

The response of a mirror to voltages is assumed to be linear and we denote by $\mathbf{N}$ the matrix defining the linear relationship between the voltages $\mathbf{u}$ applied on the mirrors and the generated correction phase $\boldsymbol{\varphi}_{cor}$:

$$\boldsymbol{\varphi}^{cor} = \mathbf{N}\mathbf{u}. \tag{4}$$

3. OPTIMAL CONTROL LAW FOR CLOSED LOOP OPERATION

What we call a closed loop is a system where the WFS are behind the mirrors and analyze the residual phase. We present the system in section 3.1 and we express in section 3.2 the temporal and spatial priors in a state space modelization. The estimator proposed in section 3.3 gives, for a given temporal sequence of measurements, the best estimate of the turbulent phase, knowing the temporal and spatial statistics of turbulence and noise. As long as we assume that the mirror response is much higher than the loop sampling frequency, it is possible to separate the control law in two parts, the estimation of the turbulent phase and the commande of the mirrors, without loosing any optimality. This is known as the Separation principle [4]. Once $\hat{\boldsymbol{\varphi}}^{tur}$ is known, the optimal commands are then given by a simple projection of $\hat{\boldsymbol{\varphi}}^{tur}$ on the mirrors [4].

Downloaded From: http://proceedings.spiedigitallibrary.org/ on 07/14/2015 Terms of Use: http://spiedl.org/terms

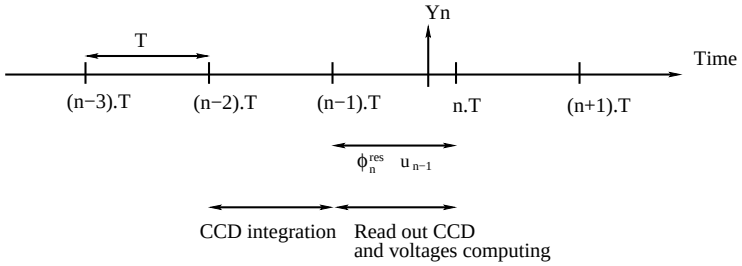

Figure 3. Temporal diagram showing the different time intervals. ϕ_n^{cor}, ϕ_n^{tur} and ϕ_n^{res} are integrated between $n-1$ and n and u_{n-1} is applied between the same period.

3.1. Closed loop basic relationships

The measurements are obtained with an exposure time T and the correction $\boldsymbol{\varphi}^{cor}(t)$ is constant between $(n-1).T$ and $n.T$, where n corresponds to the frame number. Thus the problem can be discretized using T as the sampling period. For any continuous variable $\mathbf{f}(t)$, one can associate the discrete quantity $\mathbf{f}_n$ defined as:

$$\mathbf{f}_n = \frac{1}{T}\int_{(n-1)T}^{nT} \mathbf{f}(t)dt. \tag{5}$$

The temporal diagram of the system in Fig. 3 shows how measurements and computations follow one another. If we assume that the voltage computation is done during the same time, there is a two-sampling period delay between the beginning of the integration and the application of the correction.

Let $\mathbf{N}$ be the matrix defined in section 2 and $\mathbf{u}_{n-1}$ the voltages applied between $n-1$ and n, $\mathbf{u}_{n-1}$ is linked to the correction phase $\boldsymbol{\varphi}_n^{cor}$ induced by the mirror between $n-1$ and n by the relation:

$$\boldsymbol{\varphi}_n^{cor} = \mathbf{N}\mathbf{u}_{n-1}. \tag{6}$$

It must be noted that Eq. (6) means that the mirror dynamics is neglected, as already mentioned. Vector $\mathbf{u}_n$, which is applied between n and $n+1$, should be given from the knowledghe of $\hat{\boldsymbol{\varphi}}_{n+1}^{tur}$ which minimizes:

$$\boldsymbol{\epsilon}''_{n+1} = \left\langle \left\| \boldsymbol{\varphi}_{n+1}^{tur} - \hat{\boldsymbol{\varphi}}_{n+1}^{tur} \right\|^2 \right\rangle_{\boldsymbol{\varphi},noise}. \tag{7}$$

Our prior knowledge on the turbulence evolution can be expressed as

$$\boldsymbol{\varphi}_{n+1}^{tur} = \mathbf{F}\left[\boldsymbol{\varphi}_n^{tur}, \boldsymbol{\varphi}_{n-1}^{tur}, \boldsymbol{\varphi}_{n-2}^{tur}, ...\right] + \boldsymbol{\nu}_n, \tag{8}$$

Downloaded From: http://proceedings.spiedigitallibrary.org/ on 07/14/2015 Terms of Use: http://spiedl.org/terms

where $\boldsymbol{\nu}$ is a white noise, of covariance matrix $\mathbf{C}_\nu$, and $\mathbf{F}$ is a linear function. For the simulations, we have chosen to use the following first order model:

$$\boldsymbol{\varphi}_{n+1}^{tur} = \mathbf{A}\boldsymbol{\varphi}_n^{tur} + \boldsymbol{\nu}_n. \tag{9}$$

In this model, $\mathbf{C}_\nu$ can be easily determined in order to conserve the global energy of the turbulence, hence

$$\mathbf{C}_\nu = \mathbf{C}_{\boldsymbol{\varphi}} - \mathbf{A}^T\mathbf{C}_{\boldsymbol{\varphi}}\mathbf{A}, \tag{10}$$

with $\mathbf{C}_{\boldsymbol{\varphi}}$ the covariance matrix of the turbulent phase.

With a first order model the temporal correlation function decreases exponentially. Real turbulence temporal evolution [18] could be fitted more precisely by using a higher order model.

Finally, in SO MCAO, the measurements that are used to compute $\mathbf{u}_n$ are given by:

$$\mathbf{Y}_n = \mathbf{D}\boldsymbol{\Phi}_{n-1}^{res,SO} + \mathbf{w}_n^{SO}, \tag{11}$$

$\boldsymbol{\Phi}_n^{res}$ being the residual phase in the pupil in the N_{gs} GSs directions, $\mathbf{D}$ being the interaction matrix of the system and $\mathbf{w}^{SO}$ a white noise (measurement noise). Its covariance matrix is noted $\mathbf{C}_{\mathbf{w}}^{\mathbf{SO}}$. $\boldsymbol{\Phi}^{res}$ is the residual phases in all the GS's directions. Then:

$$\mathbf{Y}_n = \mathbf{D}\left(\mathbf{M}_{\boldsymbol{\beta}}^{L,SO}\boldsymbol{\varphi}_{n-1}^{tur} - \mathbf{M}_{\boldsymbol{\beta}}^{DM,SO}\mathbf{N}\mathbf{u}_{n-2}\right) + \mathbf{w}_n^{SO}. \tag{12}$$

In the same way, we can write the expression of the measurement in LO MCAO:

$$\mathbf{Y}_n = \mathbf{D}\left(\mathbf{M}_{\boldsymbol{\beta}}^{L,LO}\boldsymbol{\varphi}_{n-1}^{tur} - \mathbf{M}_{\boldsymbol{\beta}}^{DM,LO}\mathbf{N}\mathbf{u}_{n-2}\right) + \mathbf{w}_n^{LO}. \tag{13}$$

It is also given by the difference between turbulent and correction phases, but projected in a different way. The WFSs are conjugated to different altitudes and therefore the measurement is given by the footprints of the all stars at the given altitudes. As an illustration, Fig. 2 represents the measurement footprints in SO and LO in the case of three guides stars and two LO WFSs, the first one being in the pupil plane. The $\mathbf{M}_{\boldsymbol{\beta}}^{L,SO}$ and $\mathbf{M}_{\boldsymbol{\beta}}^{DM,SO}$ matrices give the summation of the turbulent layers or of the deformable mirrors, in the three directions of the three guide stars represented in Fig. 2 left. The equivalent matrices for LO MCAO are $\mathbf{M}_{\boldsymbol{\beta}}^{L,LO}$ and $\mathbf{M}_{\boldsymbol{\beta}}^{DM,LO}$. They give the summation of the turbulent layers or deformable mirror displaced of the distance given by the footprints of the stars at the considered layer. The propagated noise $\mathbf{w}^{LO}$ or $\mathbf{w}^{SO}$ is also different and is studied in details in [3].

3.2. The linear state space modeling

A linear state space model describes the dynamical behavior of a system and its outputs (measurements) using a state space vector, whose evolution is given by a linear equation called the state equation.

In our case, the state model based on a state vector $\mathbf{X}_n$ must summarize the basic relationships of the system into the standard formulation [12]:

$$\mathbf{X}_{n+1} = \mathbf{A}_{\mathbf{1}n}\mathbf{X}_n + \mathbf{A}_{\mathbf{2}n}\mathbf{u}_n + \mathbf{V}_n, \tag{14}$$

$$\mathbf{Y}_n = \mathbf{A}_{\mathbf{3}n}\mathbf{X}_n + \mathbf{w}_n, \tag{15}$$

where $\mathbf{w}_n$ is the noise defined in Eq. (11) and $\mathbf{V}_n$ a Gaussian white noise with covariance matrix $\mathbf{C}_{\mathbf{v}}$.

If we consider that the system is stationary, the $\mathbf{A}_{\mathbf{i}n}$ matrices are time independent, $\mathbf{A}_{\mathbf{1}n} = \mathbf{A}_{\mathbf{1}}$, $\mathbf{A}_{\mathbf{2}n} = \mathbf{A}_{\mathbf{2}}$, $\mathbf{A}_{\mathbf{3}n} = \mathbf{A}_{\mathbf{3}}$, $\forall n$.

The choice of the state vector is crucial. $\mathbf{X}$ must contain all variables necessary to write the state equation (14), the measurement equation (15) and to estimate the new commands. In other words, the equations (12) for

Downloaded From: http://proceedings.spiedigitallibrary.org/ on 07/14/2015 Terms of Use: http://spiedl.org/terms

SO MCAO (or (13) for LO MCAO) and (8) must be summarized into (14) and (15) and $\mathbf{X}$ must be sufficient for estimating $\mathbf{u}$ which minimizes (7). Equations (12) or (12) implies then that $\mathbf{X}_n$ must contain $\boldsymbol{\varphi}_{n-1}^{tur}$ and $\mathbf{u}_{n-2}$. The voltages $\mathbf{u}_n$ are determined only through $\mathbf{X}_n$ so as to correct $\boldsymbol{\varphi}_{n+1}^{tur}$ (this corresponds to a prediction) . This implies that $\boldsymbol{\varphi}_{n+1}^{tur}$ must be in $\mathbf{X}_n$.

At this stage, $\mathbf{X}_n$ is composed of at least $\boldsymbol{\varphi}_{n+1}^{tur}$, $\boldsymbol{\varphi}_{n-1}^{tur}$ and $\mathbf{u}_{n-2}$. To be able to write the evolution equation for $\boldsymbol{\varphi}_{n+1}^{tur}$, $\boldsymbol{\varphi}_{n}^{tur}$ must be in the state vector too, and, as $\mathbf{u}_{n-2}$ must be kept in memory, $\mathbf{u}_{n-1}$ is also contained in $\mathbf{X}_n$.

$\mathbf{X}_n$ needs also to contain all the $\boldsymbol{\varphi}_{n-i}^{tur}$ used in Eq. (8). For the first order model considered in our simulations, we only need $\boldsymbol{\varphi}_{n}^{tur}$, which is anyway already included in $\mathbf{X}_n$.

For a first order evolution model, the state vector is then: $\mathbf{X}_n = \begin{pmatrix} \boldsymbol{\varphi}_{n+1}^{tur} \\ \boldsymbol{\varphi}_{n}^{tur} \\ \boldsymbol{\varphi}_{n-1}^{tur} \\ \mathbf{u}_{n-1} \\ \mathbf{u}_{n-2} \end{pmatrix}$ and the state model is:

$$\mathbf{X}_{n+1} = \begin{pmatrix} \mathbf{A} & 0 & 0 & 0 & 0 \\ \mathbf{Id} & 0 & 0 & 0 & 0 \\ 0 & \mathbf{Id} & 0 & 0 & 0 \\ 0 & 0 & 0 & 0 & 0 \\ 0 & 0 & 0 & \mathbf{Id} & 0 \end{pmatrix} \mathbf{X}_n + \begin{pmatrix} 0 \\ 0 \\ 0 \\ \mathbf{Id} \\ 0 \end{pmatrix} \mathbf{u}_n + \begin{pmatrix} \boldsymbol{\nu}_n \\ 0 \\ 0 \\ 0 \\ 0 \end{pmatrix} \tag{16}$$

$$\mathbf{Y}_n = \mathbf{D} \begin{pmatrix} 0 & 0 & \mathbf{M}_{\boldsymbol{\beta}}^{L,SO} & 0 & -\mathbf{M}_{\boldsymbol{\beta}}^{DM,SO}\mathbf{N} \end{pmatrix} \mathbf{X}_n + \mathbf{w}_n^{SO} \tag{17}$$

for a SO MCAO. Obviously, for a LO MCAO system, the first equation, known as the evolution equation does not change and the second one, the measurement equation, becomes:

$$\mathbf{Y}_n = \mathbf{D} \begin{pmatrix} 0 & 0 & \mathbf{M}_{\boldsymbol{\beta}}^{L,LO} & 0 & -\mathbf{M}_{\boldsymbol{\beta}}^{DM,LO}\mathbf{N} \end{pmatrix} \mathbf{X}_n + \mathbf{w}_n^{LO} \tag{18}$$

3.3. Kalman filter and feedback control

If a system can be described by a linear state model, the optimal estimation of $\mathbf{X}_{n+1}$ knowing the measurements $\{\mathbf{Y}_0, ..., \mathbf{Y}_n\}$ is provided by a Kalman filter, which corresponds to the recursive estimation

$$\hat{\mathbf{X}}_{n+1/n} = \mathbf{A_1}\hat{\mathbf{X}}_{n/n-1} + \mathbf{A_2}\mathbf{u}_n + \mathbf{A_1}\mathbf{H}_n(\mathbf{Y}_n - \mathbf{A_3}\hat{\mathbf{X}}_{n/n-1}), \tag{19}$$

where $\hat{\mathbf{X}}_{n+1/n}$ is the prediction of $\mathbf{X}_{n+1}$ using $\{\mathbf{Y}_0, ..., \mathbf{Y}_n\}$. $\mathbf{H}_n$ is called the observator gain and is doing the trade-off between priors and measurements. It is equal to:

$$\mathbf{H_n} = \mathbf{C}_{n/n-1}\mathbf{A_3}^T \left(\mathbf{A_3}\mathbf{C}_{n/n-1}\mathbf{A_3}^T + \mathbf{C_w}\right)^{-1}, \tag{20}$$

with $\mathbf{C_w}$ the matrix covariance of the noise and $\mathbf{C}_{n/n-1}$ the matrix covariance of the state vector estimation error, predicted for the instant n at the instant $n-1$. $\mathbf{C}_{n/n-1}$ is computed by solving the Ricatti equation [10]:

$$\mathbf{C}_{n+1/n} = \mathbf{A_1}\mathbf{C}_{n/n-1}\mathbf{A_1}^T + \mathbf{C_v} - \mathbf{A_1}\mathbf{C}_{n/n-1}\mathbf{A_3}^T \left(\mathbf{A_3}\mathbf{C}_{n/n-1}\mathbf{A_3}^T + \mathbf{C_w}\right)^{-1} \mathbf{A_3}\mathbf{C}_{n/n-1}\mathbf{A_1}^T. \tag{21}$$

One must note that, as we already said, there is a delay between the measurement and the correction. This means that it is necessary to make a prediction of the evolution of the turbulent phase. The approach we propose makes this predicition by using the equation of evolution of the turbulence, induced by Eq. (16). This is why the state vector $\mathbf{X}_n$ contains $\boldsymbol{\varphi}_{n+1}^{tur}$. The estimation of $\mathbf{X}_n$ therefore implicitly includes this prediction step.

The voltages are then given by:

$$\mathbf{u}_n = \mathbf{P}_{[\boldsymbol{\alpha};DM]}\hat{\boldsymbol{\varphi}}_{n+1/n}^{tur}. \tag{22}$$

with $\mathbf{P}_{[\boldsymbol{\alpha};DM]}$ the projector given in [1].

Downloaded From: http://proceedings.spiedigitallibrary.org/ on 07/14/2015 Terms of Use: http://spiedl.org/terms

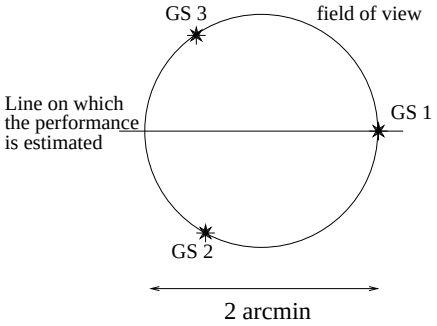

Figure 4. Illustration of the guide stars geometry and of the directions on which the performances are estimated.

4. SIMULATIONS, RESULTS AND INTERPRETATIONS

We now quantify the gain brought by this new approach in SO MCAO using numerical simulations.

4.1. Simulation conditions

We first present the turbulence and system simulation conditions. The results presented here correspond to a 8m class telescope observing in the near infrared (2.2 μm). We use for the wave front sensing three GSs located on the vertices of an equilateral triangle inscribed in a field of view of 2 arcmin, as shown in Fig. 4. The SNR on Shack-Hartmann measurements is equal to 10.

We consider a two-layer atmosphere. The layer altitudes are 500 meters and 10 kilometers and the strength of the turbulence is 80% in the lower layer and 20% in the higher one. The global $\frac{D}{r_0}$ is set to 9. For a 8m telescope diameter, $r_0 = 0,89$m at $2,2\mu m$ and $\theta_0 =$ at $2,2\mu m$, which is representative of astronomical sites.

We created a turbulent phase composed of 13 radial orders in the first layer and 26 in the second one. The phase is generated layer by layer using the same first order AR process which is used to modelyze the turbulence evolution in model on which is based the Kalman filter. For generating the turbulent phase, the matrix $\mathbf{A}$ in equation (9) has been chosen diagonal and its elements adjusted to respect the characteristics of a turbulence of wind speed $\frac{v}{D} = 2$Hz.

We have simulated the SO MCAO system using the state model. The sampling frequency is 100 Hz and the delay of the loop is two sampling periods. The WFS can measure 13 radial orders of Zernike polynomials and the noise on the measurements is representative of a 12×12 microlenses Shack-Hartmann WFS. We use two mirrors conjugated at 500 meters and 10 kilometers, that is, on the turbulent layers themselves and which can correct 13 radial orders for the lower one and 26 radial orders of Zernike polynomials for the higher one.

We compute the variances of residual phase in different directions. In this computation, we take into account the Noll residual variance.

We also present the Strehl Ratio [SR] which is approximated as the Coherent Energy $\exp(-\sigma^2_{res})$. This is a good approximation for good corrections.

Downloaded From: http://proceedings.spiedigitallibrary.org/ on 07/14/2015 Terms of Use: http://spiedl.org/terms

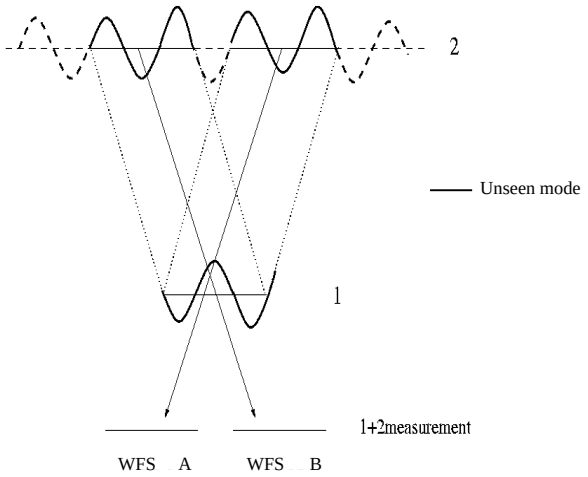

Figure 5. Illustration of the concept of unseen modes.

4.2. Unseen modes in MCAO

Before presenting the simulation results, we should remind what we call unseen modes. An unseen mode is a mode that is not measured by the WFS [15–17]. An example of unseen modes in MCAO is shown in Fig. 5. This figure represents two wavefronts at different altitudes which compensate each other exactly in the measurements directions. The WFSs then measure nothing. The problem is that the wavefronts do not compensate and degrade the image quality in the other directions. The more the GS are distant and the more unseen modes contain turbulent energy. This is the reason why unseen modes must be taken into account, because filtering out high energy unseen modes, degrades considerably the image quality.

4.3. Results and interpretations

We compare the Kalman filter performance in the SO MCAO case with a new approach, the "Multiconjugate Optimized Modal Gain Integrator" [MOMGI], which is a generalization to the MCAO of the OMGI approach in classical AO [13, 14]. The gains of the integrator are optimized mode by mode in the basis of the eigen modes of $\left(\mathbf{DM}_{\boldsymbol{\beta}}^{DM,SO}\mathbf{N}\right)^T\left(\mathbf{DM}_{\boldsymbol{\beta}}^{DM,SO}\mathbf{N}\right)$ so that the residual variance is minimized mode by mode. There are 482 eigen modes. We recall that $\mathbf{M}_{\boldsymbol{\beta}}^{L,SO}$ is the matrix that performs the summation on the turbulent layers in all directions $\boldsymbol{\beta}$. In this basis, the modes whose eigen values are the lower are badly seen and the modes whose eigen values are 0 are unseen. The lower the eigen value, the lower the gain on this mode. The optimized gains in this basis are plotted in Fig. 6. One must note that, as the size of $\mathbf{DM}_{\boldsymbol{\beta}}^{DM,SO}\mathbf{N}$ is 482×312, there are at least 170 zeros in the eigen values, thus at least 170 zero gains.

As the gains decrease with the eigen values, the unseen modes are filtered out by the MOMGI approach, while the Kalman filter estimates them by using spatial *a priori* knowledge. As we know from previous works [8], the estimation of unseen modes can be very critical for the performance of the system in the field of view between the guide stars. We expect then a significative gain for the Kalman approach.

The gains of the MOMGI estimator have been thresholded to 0.5 to ensure stability.

We present in Fig. 7 the Strehl Ratio along a line joining the center of the GSs triangle and one of the GSs (as shown in Fig. 4) for the two approaches and for the Classical AO OMGI case. The difference of performance observed on the GS between the Kalman approach and the others is due to the temporal error. It is the same kind of improvement than the one observed in classical AO [1, 2] and is due to the fact that the Kalman approach we propose provides a temporal prediction. The best performance is obtained for each case on the GS and degrades away from it. Our approach provides a noticeable improvement compared to the MOMGI and a better interpolation between the guide stars. The difference between the two corresponds to some percents of SR on

Downloaded From: http://proceedings.spiedigitallibrary.org/ on 07/14/2015 Terms of Use: http://spiedl.org/terms

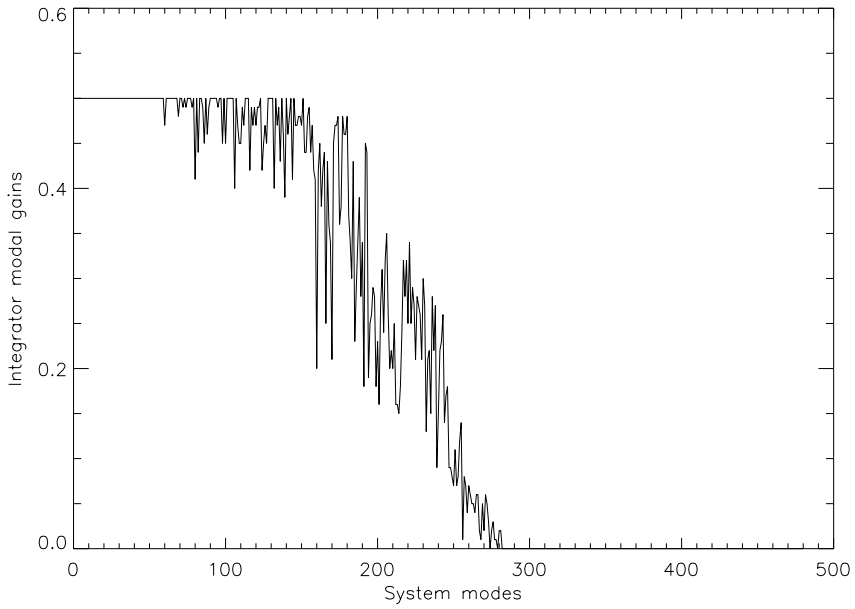

Figure 6. The optimized modal gains in the SO MCAO case, in the basis of the eigen modes of $(\mathbf{M}_{\boldsymbol{\beta}}^{L,SO})^T\mathbf{M}_{\boldsymbol{\beta}}^{L,SO}$.

the GS and ten precents on the border of the field of view. This difference is essentially due to the ability of the Kalman filter to estimate unseen modes.

We have also presented in Fig. 8 the variance of the residual phase on the pupil versus the Zernike mode in two directions, the GS direction and the center of the field of view. The deterioration of the integrator performance in the center of the field of view is obvious and is due to the presence of unseen modes.

5. CONCLUSION

We have proposed in this paper an optimal closed loop control which can be applied to SO and LO Multiconjugate Adaptive Optics. It is based on a linear state space model with a Kalman observator. This approach gives an optimal estimation of the turbulence in closed loop. It incorporates both spatial and temporal information on the turbulent phase, as well as information on the noise statistics.

We have shown through a numerical simulation that this approach gives much better results in SO MCAO than other methods, thanks to its ability to estimate unseen modes.

The adaptability of such a physical-model-based optimal control allows to adapt the control law to a SO or LO MCAO system by changing only the measurement equation on the state-space model. This demonstrates once again the interest of this approach that could allow to take into account and then correct at least partially any physical effect as long as it can be explicitly expressed in a linear state-space model.

Acknowledgements

The authors thank L.M. Mugnier and T. Fusco for fruitfull discussions.
This work has been partially funded by the European Research and Training Network *Adaptive Optics for Extremely Large Telescopes*, Contract HPRN-CT-2000-00147.

Further informations: Email: leroux@arcetri.astro.it; Phone: +39 055 2752281; Fax: +39 055 220039

Downloaded From: http://proceedings.spiedigitallibrary.org/ on 07/14/2015 Terms of Use: http://spiedl.org/terms

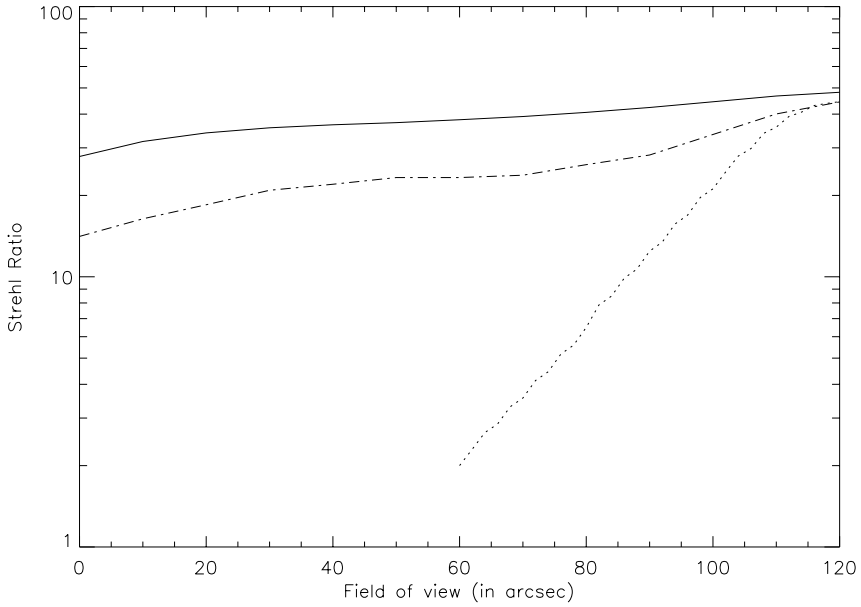

Figure 7. Comparison between the Kalman approach [solid line], the MOMGI approach [mixed line] and the Classical AO case (dotted line). The Strehl Ratio is plotted versus the position in the FOV in arcseconds.

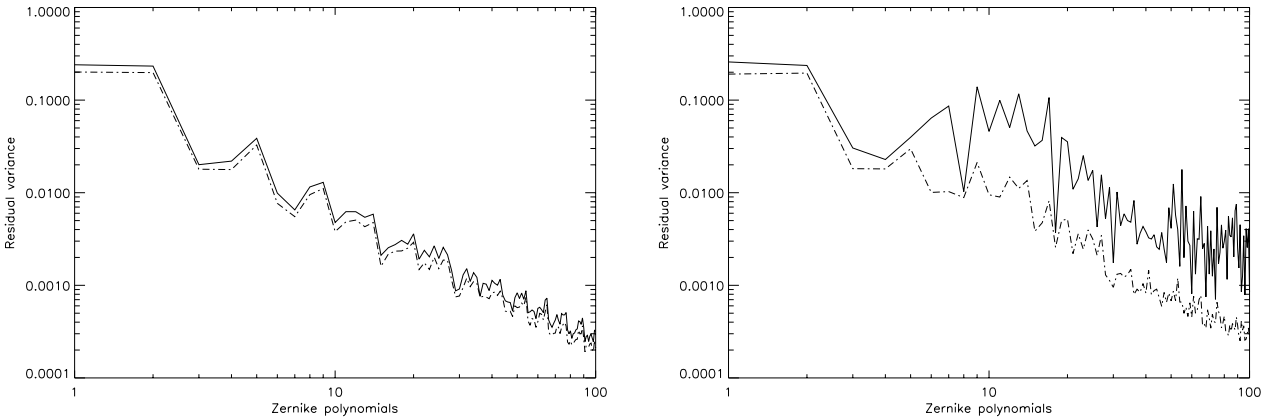

Figure 8. The residual phase variance as a function of the Zernike mode for the Kalman approach [mixed line] and the MOMGI approach [solid line]. Left= on a Guide Star. Right= on the center of the field of view.

Downloaded From: http://proceedings.spiedigitallibrary.org/ on 07/14/2015 Terms of Use: http://spiedl.org/terms

REFERENCES

1. B. Le Roux, J.-M. Conan, C. Kulcsàr, H.-F.Raynaud, L.M. Mugnier, T. Fusco, "Optimal control law for Multiconjugate Adaptive Optics," in *Adaptive Optical System Technologies II*, D. B. Peter Wizinowich, ed., Proceedings of SPIE **4839,** 878–889 (2003).
2. C. Petit, F. Quiros Pacheco, J.-M. Conan, C. Kulcsàr, H.F. Raynaud, T. Fusco, " Kalman filter-based control loop for MCAO: performance and robustness," in *Advancements in Adaptive Optics*, D. Bonaccini, B. L. Ellerbroek, R. Ragazzoni, eds., Proceedings of SPIE **5490,** (2004, Glasgow).
3. D. Bello, J.-M. Conan, G. Rousset, R. Ragazzoni, "Signal to noise ratio of layer-oriented measurements for multiconjugate adaptive optics", A&A, **410** 1101–1106 (2003)
4. B. Le Roux, J.-M. Conan, C. Kulcsàr, H.-F.Raynaud, L.M. Mugnier, T. Fusco, "Optimal control law for classical and multiconjugate Adaptive Optics," J. Opt. Soc. Am. A. **21(7)** 1261–1276 (2004)
5. J. Beckers, "Increasing the size of the isoplanatic patch with multiconjugate adaptive optics.," in *Very Large Telescopes and their Instrumentation*, e. Ulrich, M.-H., ed.,**2,** 693–703 (1988).
6. M. Tallon, R. Foy, and J. Vernin, "3-d wavefront sensing and multiconjugate adaptive optics," in *Progress in Telescope and Instrumentation Technologies*, M.-H. Ulrich, ed., ESO Conference and Workshop Proceedings **42,** 517–521 (1992).
7. B. L. Ellerbroek, "First-order performance evaluation of adaptive-optics systems for atmospheric-turbulence compensation in extended-field-of-view astronomical telescopes.," J. Opt. Soc. Am. A. **11(2),** 783–805 (1994).
8. T. Fusco, J.-M. Conan, G. Rousset, L. Mugnier, and V. Michau, "Optimal wavefront reconstruction strategies for multiconjugate adaptive optics.," J. Opt. Soc. Am. A 18 (2001).
9. R. Ragazzoni, "No laser guide stars for adaptive optics in giant telescopes.," *Astron. Astrophys. Suppl. Ser.* **136,** 205–209 (1999).
10. H. V. Trees, *Detection, Estimation and Modulation Theory, Part I* (Wiley, New York, 1968).
11. A. Papoulis, *Probability, Random Variables and Stochastic Processes, 3rd ed.* (McGraw-Hill, New York, 1991).
12. B. Anderson and J. Moore, *Optimal control, linear quadratic methods* (London: Prentice Hall, 1989).
13. E. Gendron and P. Lena, "Astronomical Adaptive Optics I. Modal control optimization," Astronomy and Astrophysics **291,** 337–347 (1994).
14. E. Gendron and P. Lena, "Astronomical Adaptive Optics II. Experimental results of an optimize modal control," Astronomy and Astrophysics **111,** 153–167 (1994).
15. T. Fusco, J.-M. Conan, V. Michau, G. Rousset, and F. Assémat, "Multi-conjugate adaptive optics: Comparison of phase reconstruction approaches for large field of view.," in *Optics in Atmospheric Propagation and Adaptive Systems VI*, e. In Wizinowich, P. L., ed., Proc. Soc. Photo-Opt. Instrum. Eng. 4167 (2000).
16. M. Le Louarn, "Multiconjugate Adaptive Optics: a PSF study," in *Beyond Conventional Adaptive Optics*, S. E. R. Ragazzoni, ed., ESO Conference and workshop proceedings **58,** 217–222 (2001).
17. E. Diolaiti, C. Arcidiacono, R. Ragazzoni, and E. Fedrigo, "Identification and rejection of waffle modes in layer-oriented adaptive optics," in *Adaptive Optical System Technologies II*, D. B. Peter Wizinowich, ed., Proceedings of SPIE **4839,** 1001–1010 (2003).
18. J.-M. Conan, G. Rousset, and P.-Y. Madec, "Wave-front temporal spectra in high-resolution imaging through turbulence," J. Opt. Soc. Am. A **12,** 1559–1570 (1995).
19. R. Noll, "Zernike polynomials and atmospheric turbulence," J. Opt. Soc. Am. A **66,** 207–211 (1976).

Downloaded From: http://proceedings.spiedigitallibrary.org/ on 07/14/2015 Terms of Use: http://spiedl.org/terms